Journal of Proteomics 283–284 (2023) 104928

Contents lists available at ScienceDirect

Journal of Proteomics

journal homepage: www.elsevier.com/locate/jprot

Proteomic analysis of murine *Tsc1*-deficient neural stem progenitor cells

Elisabetta Chiaradia [a,1], Ingrid Miller [b,*,1], Giovanni Renzone [c], Alessia Tognoloni [a], Alice Polchi [d], Federico De Marco [e], Brunella Tancini [d,**], Andrea Scaloni [c], Alessandro Magini [f]

[a] *Biochemistry and Proteomics Laboratory, Department of Veterinary Medicine, University of Perugia, Perugia, Italy*
[b] *Institute of Medical Biochemistry, University of Veterinary Medicine Vienna, Vienna, Austria*
[c] *Proteomics, Metabolomics & Mass Spectrometry Laboratory, ISPAAM, National Research Council, Portici, Italy*
[d] *Department of Chemistry, Biology and Biotechnology, University of Perugia, Perugia, Italy*
[e] *Research and Advanced Technologies Department, IRCCS Regina Elena National Cancer Institute, Rome, Italy*
[f] *Associazione Sclerosi Tuberosa, O.N.L.U.S., Rome, Italy*

ARTICLE INFO

Keywords:
Tuberous sclerosis complex
Proteomics
Neural stem progenitor cells
Protein biomarkers

ABSTRACT

Tuberous sclerosis complex (TSC) is a rare, multisystem genetic disorder that leads to the development of benign tumors in multiple organs and neurological symptoms. TSC clinical manifestations show a great heterogenicity, with most patients presenting severe neuropsychiatric and neurological disorders. TSC is caused by loss-of-function mutations in either *TSC1* or *TSC2* genes, leading to overexpression of the mechanistic target of rapamycin (mTOR) and, consequently, abnormal cellular growth, proliferation and differentiation as well as to cell migration defects. Beside the growing interest, TSC remains a disorder poorly understood, with limited perspectives in the field of therapeutic strategies. Here we used murine postnatal subventricular zone (SVZ) neural stem progenitor cells (NSPCs) deficient of *Tsc1* gene as a TSC model to unravel novel molecular aspects of the pathophysiology of this disease. 2D-DIGE-based proteomic analysis detected 55 differently represented spots in *Tsc1*-deficient cells, compared to wild-type counterparts, which were associated with 36 protein entries after corresponding trypsinolysis and nanoLC-ESI-Q-Orbitrap-MS/MS analysis. Proteomic results were validated using various experimental approaches. Bioinformatics associated differently represented proteins with oxidative stress and redox pathways, methylglyoxal biosynthesis, myelin sheath, protein S-nitrosylation and carbohydrate metabolism. Because most of these cellular pathways have already been linked to TSC features, these results were useful to clarify some molecular aspects of TSC etiopathogenesis and suggested novel promising therapeutic protein targets.

Significance: Tuberous Sclerosis Complex (TSC) is a multisystemic disorder caused by inactivating mutations of *TSC1* or *TSC2* genes, which induce overactivation of the mTOR component. The molecular mechanisms underlying the pathogenesis of TSC remain unclear, probably due to complexity of mTOR signaling network. To have a picture of protein abundance changes occurring in TSC disorder, murine postnatal subventricular zone (SVZ) neural stem progenitor cells (NSPCs) deficient of *Tsc1* gene were used as a model of disease. Thus, *Tsc1*-deficient SVZ NSPCs and wild-type cells were comparatively evaluated by proteomics. This analysis evidenced changes in the abundance of proteins involved in oxidative/nitrosative stress, cytoskeleton remodelling, neurotransmission, neurogenesis and carbohydrate metabolism. These proteins might clarify novel molecular aspects of TSC etiopathogenesis and constitute putative molecular targets for novel therapeutic management of TSC-related disorders.

Abbreviations: AGEs, advanced glycation end-products; ALDO, fructose-bisphosphate aldolase; CA, carbonic anhydrase; FABP7, fatty acid-binding protein, brain; FC, fold change; GFAP, glial fibrillary acidic protein; GLO1, glyoxalase1; hnRNPL, heterogeneous nuclear ribonucleoprotein L; MG, methylglyoxal; mTOR, mechanistic target of rapamycin; mTORC1, mTOR complex 1; NME1, nucleoside diphosphate kinase A; NSPCs, neural stem progenitor cells; SEGAs, subependymal giant cell astrocytomas; SENs, subependymal nodules; SVZ, subventricular zone; TPI, triosephosphate isomerase; TSC, tuberous sclerosis complex; $Tsc1^{ko}$, *Tsc1*-deficient NSPCs..

* Correspondence to: Ingrid Miller, Institute of Medical Biochemistry, University of Veterinary Medicine Vienna, Veterinärplatz 1, Vienna 1210, Austria.
** Correspondence to: Brunella Tancini, Department of Chemistry, Biology and Biotechnology, University of Perugia, Perugia 06126, Italy.
E-mail addresses: ingrid.miller@vetmeduni.ac.at (I. Miller), brunella.tancini@unipg.it (B. Tancini).
[1] Both authors contributed equally to this work

https://doi.org/10.1016/j.jprot.2023.104928
Received 1 December 2022; Received in revised form 16 April 2023; Accepted 3 May 2023
Available online 18 May 2023

1. Introduction

Tuberous sclerosis complex (TSC) is a rare, multisystem autosomal dominant disorder that causes the development of benign tumors in the brain and other organs, as well as various neurological symptoms. In most cases, TSC is caused by loss-of-function mutations in either *TSC1*or *TSC2* genes encoding for hamartin and tuberin, respectively; additional cases (about 10% of total) not related to mutations in *TSC1* or *TSC2* genes were also identified [1]. Mutations in *TSC1* or *TSC2* genes lead to the hyperactivation of the mechanistic target of rapamycin (mTOR) [2–5], which is a Ser/Thr protein kinase related to the PI3K-protein kinase family, having a central role in regulating cell growth and metabolism in response to physiological conditions and environmental cues [6–8]. It is also involved in various cellular processes that directly impact differentiation and migration of neuronal cells in the central nervous system (CNS) [9].

TSC is characterized by a wide spectrum of clinical manifestations. In general, most TSC patients present severe neuropsychiatric and neurological disorders including epilepsy, developmental delay and autism. Moreover, mTOR hyperfunction results in the development of benign tumors, known as hamartomas, in multiple organs, including brain, kidneys, skin, lung and heart [10,11]. TSC brain lesions mainly consist in cortical tubers, subependymal nodules (SENs) and subependymal giant cell astrocytomas (SEGAs). Cortical tubers are characterized by dysplastic neurons, multinucleated giant cells and loss of normal cortical lamination that result from abnormalities during the development of the cerebral cortex [12]. SENs are asymptomatic lesions that line the lateral and third ventricles, and contain enlarged neurons, glia and giant cells [10]. In some cases, SENs can evolve into SEGAs, which are larger lesions expressing both neuronal and astrocytes markers [13]. Even if SEGAs are benign astrocytomas, they can block cerebrospinal fluid drainage at the foramen of Monro causing obstructive hydrocephalus and death [14]. Studies on TSC animal models have shown that neural progenitor cells are the source of brain lesions, which result from abnormalities on cell proliferation, differentiation and migration during neurogenesis [15–18]. Severe impairments in neuronal differentiation and development as well as increased production of astro-glial cells have also been observed in human neural models of TSC [19]. In agreement with neurodevelopmental alterations associated with TSC, many studies support a role of altered mTOR function in the impaired regulation of various processes of neurogenesis and brain development/activity [5,20]. It has been widely proven that mTORC1 hyperactivation causes profound changes in the neuronal differentiation processes, leading to reduced self-renewal of neural stem cells and premature differentiation versus the astrocyte lineage, precluding neuronal and oligodendroglial cell maturation [17,21]. Noteworthy, break of oligodendrocyte maturation results in hypomyelination, which is another peculiar neurological manifestation of TSC. mTOR signaling pathways also play a critical role in proper neuron migration, supporting the defect in migration observed in both TSC mouse models and patients [16,18,22,23]. In particular, hyperactivation of mTORC1 in neural stem progenitor cells (NSPCs) of postnatal subventricular zone (SVZ) halted neuronal migration to the olfactory bulb and resulted in abnormal neuron morphology and circuit formation [16,24].

Consistent with the central role of mTOR hyperactivation in disease onset, pharmacological treatments of TSC are mainly focused on the use of mTOR inhibitors, such as everolimus or sirolimus [25]. Recently, the promising results obtained by using a GABA transaminase inhibitor [11] and cannabidiol [26] for the treatment of some TSC-related disorders have highlighted the need of novel therapeutic strategies to cure the different pathological manifestations of this disease.

Because of the high complexity of mTOR signaling network and the numerous cellular processes involved, the molecular mechanisms underlying the pathophysiology of TSC are still not fully understood. In the last years, proteomic studies have been contributing to elucidate some molecular aspects of CNS lesions and neurological manifestations of TSC. In particular, preliminary proteomic characterizations of some different brain areas of human patients with *TSC1* mutations [27] and of *Tsc1*-knockout mice have been performed [28,29]. Although the promising results evidenced protein alterations and cellular pathway dysregulation linked to TSC clinical manifestations, further studies are needed to define the effects of mTOR hyperactivation and their implications in the disease onset.

In this study, we have performed an original proteomic analysis of a TSC-related cellular model using murine postnatal *Tsc1*-deficient SVZ NSPCs. These cells well recapitulate the main features of TSC neural stem cells including mTORC1 activation, the formation of abnormally enlarged astrocytes-like cells and reduced migration ability [3]. Therefore, this cellular model can be considered suitable to carry out a study aimed to characterize TSC neural stem cells at the proteomic level. Changes in the protein abundance due to the hyperactivated mTOR signaling have been evidenced. Furthermore, functional enrichment and network analyses evidenced the cellular processes and molecular pathways that could be involved in TSC disease.

2. Materials and methods

2.1. Murine $Tsc1^{ko}$ cell line generation and analysis

The TSC cell model was obtained as reported by Magini and coworkers [3]. Briefly, *Tsc1*-deficient NSPCs ($Tsc1^{ko}$) were obtained from NSPCs of the brain SVZ of six-week-old $Tsc1^{wt}$ conditional mice, which have loxP sites flanking exons 17 and 18 of the *Tsc1* allele [3], by transfection with GFP-Cre plasmid vector (Addgene) and using the Nucleofector™ kit (Lonza), according to the manufacturer's procedure. After transfection, GFP-expressing neurospheres were singularly recovered, dissociated into single cells with Accutase (Gibco), plated at 10×10^4 cells/cm^2 and propagated at 37 °C in humid air with 5% CO_2 in Complete NeuroCult™ NSC Proliferation Medium (NeuroCult medium; Stem Cell Technologies) supplemented with 40 ng/mL human β-FGF2 (Thermo Scientific) and 40 ng/mL human EGF (Thermo Scientific). *Tsc1* gene deletion (exons 17 and 18) was evaluated by PCR and $Tsc1^{ko}$ clones were successively analyzed by immunoblotting, as previously reported [3].

Differentiation of both $Tsc1^{wt}$ and $Tsc1^{ko}$ cells was performed by culturing cells in pre-coated matrigel six-well plates, according to the manufacturer's procedure (Matrix growth factor reduced; Corning) [3]. NSPCs were incubated in NeuroCult medium containing both 40 ng/mL β-FGF2 and EGF, for 24 h. After this time, the cells were maintained in 10 ng/mL β-FGF2 for additional 3 days, and then switched to DMEM/F12 (GIBCO) medium containing 2% FBS (GIBCO).

Cell viability was estimated by trypan blue assay by using automatic cell counter (Countess Automated Cell Counter; Thermo Scientific).

2.2. Immunofluorescence analysis

Immunofluorescence analysis was performed according to Magini and coworkers [3]. Briefly, NSPCs were plated on matrigel pre-coated 12 mm round glass coverslips at a density of 15,000 cells/cm^2 and incubated in NeuroCult medium containing both 40 ng/mL β-FGF2 and EGF, for 24 h. After a fixing step using 4% v/v paraformaldehyde in Dulbecco's phosphate-buffer saline (DPBS) and a blocking step in DPBS-containing 5% v/v FBS, 0.3% v/v Triton X-100, for 1 h at room temperature, the glass coverslips were incubated for 1 h in antibody solution (DPBS, 1% w/v BSA, 0.3% v/v Triton X-100) with primary antibody: anti-glial fibrillary acidic protein (GFAP; 1:300, Stemcell Technologies); anti-nestin (1:200, Stem Cell Technologies); anti-phospho-S6 ribosomal protein (S235/236) (1:100, Cell Signaling) or Alexa FluorR488 Phalloidin (1:1000, Thermo Fisher Scientific). After incubation with secondary antibodies, namely donkey anti-rabbit IgG Alexa FluorR488/594 or donkey anti-mouse IgG Alexa FluorR594 (Thermo Fisher Scientific), for 1 h at room temperature, coverslips were mounted on glass slides

using Vectashield with DAPI (Vector Laboratories Inc). Fluorescence microscopy analysis was performed using a Nikon TE2000 microscope (Nikon Instruments S.p.A, Florence, Italy) through a 60× oil immersion objective; the image processing was performed using Adobe-Photoshop CS software (Adobe Systems Incorporated).

2.3. Proteomic analysis

2.3.1. Protein extraction and two-dimensional differential in gel electrophoresis (2D-DIGE)

Cells were collected, washed twice in PBS and lysed in 10 mM Tris-HCl pH 7.5, 100 mM NaCl, 1 mM EDTA, 1 mM EGTA, 1% v/v Triton-X 100, 10% v/v glycerol, 0.1% w/v SDS, 0.5% w/v Na-deoxycholate for 40 min, with vortexing for 2–3 s every 10 min. The supernatant obtained after centrifugation (10.000 ×*g*, 15 min, 4 °C) was dialysed by using the Plus One Mini Dialysis Kit system (molecular mass cut off 1 kDa, GE Healthcare Life Sciences, Amersham, UK) against DIGE labelling buffer (8 M urea, 4% w/v CHAPS, 30 mM Tris-HCl pH 8.5) for 4 h at room temperature. Protein concentration was measured using Bradford assay [30], using homemade reagent and BSA as standard.

Two-dimensional differential in gel electrophoresis (2D-DIGE) was performed using 3 different cell pools of $Tsc1^{ko}$ and $Tsc1^{wt}$ cells obtained mixing 4 different cell cultures, respectively. Fluorescent labelling of proteins was carried out with a CyDye DIGE Fluor Minimal dye labelling kit (GE Healthcare); two-dimensional electrophoresis was carried out according to Miller [31]. In short, Cy2 was used for the internal standard (a pool of all samples), while Cy3 and Cy5 were used for $Tsc1^{ko}$ and $Tsc1^{wt}$ samples, respectively. This included reverse labelling for all samples, based on manufacturer's recommendations, and the labelling ratio was 8 nmol dye/mg protein. Twenty-five μg of Cy3 and of Cy5 labelled samples were mixed with 25 μg of internal standard (Cy2) and diluted with rehydration buffer (8 M urea, 4% w/v CHAPS, 13 mM DTT, 1% ampholytes). Immobilized pH gradient strips pH 3–10, linear, 11 cm strips (Serva #43031.01) were passively rehydrated for 5 h; samples were applied by anodic cup-loading. The first dimensional separation was performed in a Multiphor II electrophoresis system (GE Healthcare). After isoelectric focusing, the proteins were reduced and alkylated, incubating the strip for 10 min in an equilibration buffer (50 mM Tris-HCl pH 6.8, 6 M urea, 30% v/v glycerol, 2% w/v SDS) containing 130 mM DTT, followed by a treatment in the same buffer containing 135 mM iodoacetamide, for 5 min. The second dimensional SDS-PAGE was carried out in 140 × 140 × 1.5 mm gradient gels (T = 10–15%, C = 2.7%) in a Hoefer SE600 system (Hoefer Scientific Instruments, San Francisco, CA, USA). Images were captured on a Typhoon RGB. Quantitation of the fluorescence intensity of the protein spots and evaluation including statistical analyses were carried out using the software DeCyder V5.02 software (GE Healthcare). Statistically significantly altered protein spots ($P < 0.05$, Student's *t*-test) with more than ± 1.5-fold changes (FC) were selected for MS-based protein identification.

2.3.2. Protein identification

Selected spots were visualized by silver staining, manually picked from the gels using pipette tips or a scalpel and washed with water. Those spots of interest were *in-gel* reduced with dithiothreitol, S-alkylated with iodoacetamide, and hydrolyzed with trypsin [32]. Peptide mixtures were desalted/concentrated with μZip-TipC18 devices (Millipore, USA) and analyzed using a nanoLC-ESI-Q-Orbitrap-MS/MS system consisting of a Q-ExactivePlus Orbitrap mass spectrometer equipped with a Nanospray Flex ion source (Thermo Fisher Scientific, USA) connected to an UltiMate 3000 RSLC nano-liquid chromatographer (Dionex, USA) [33]. Protein digests were separated on an Acclaim PepMap™ RSLC C18 column (15 cm-length x 75 μm inner diameter, 2 μm particles, 100 Å pore size; Thermo Fisher Scientific, USA) using a gradient of solvent A (0.1% v/v formic acid in H_2O) to solvent B (80% acetonitrile, 20% H_2O, 0.1% formic acid, v/v/v), at a total flow rate of 300 nL/min. A linear gradient started 20 min after sample loading; eluent B ramped from 3% to 40% v/v over 40 min, and from 40% to 80% v/v over 5 min. The mass spectrometer operated in data-dependent scan mode, allowing the acquisition of all MS spectra in positive ionization mode within a scan range of *m/z* 375–1500. A nominal resolution of 70,000 in full scan MS was applied. MS/MS analyses were performed by higher collision energy fragmentation (HCD) on the eight most abundant ions from the preceding full scan, setting a dynamic exclusion duration of 30 s. MS/MS spectra were acquired in the scan range of *m/z* 110–2000, with a nominal resolution of 17,500. Isolation window and normalized collision energy were set at *m/z* 1.2 and 28%, respectively. Automatic gain control target and maximum ion injection time were set to 50,000 and 110 ms, respectively. Precursor ions, both singly charged and with more than six charges, were excluded from the fragmentation.

For protein identification, MASCOT software (v. 2.2.06, Matrix Science, UK) was used to search raw data from nanoLC-ESI-Q-Orbitrap-MS/MS analyses against an UniProtKB protein database (04/2022 release, 566,996 total entries), selecting *Mus musculus* as a taxonomy and common protein contaminants, as human keratins, trypsin, and others. Database searches were carried out allowing carbamidomethylation of cysteines as fixed protein modification and oxidation of methionines, deamidation of Asn/Gln and pyroglutamate cyclization from N-terminal Gln as variable modification, a mass tolerance value of 20 ppm for parent ions and of 0.05 Da for MS/MS fragment ions, trypsin as proteolytic enzyme, and a maximum of 2 missed cleavages. All other parameters were kept as default. At least two sequenced peptides with an individual peptide expectation value ≤0.01, corresponding to a confidence level for peptide attribution ≥99%, determined the identification of protein candidates. Decoy databases were used to calculate the false discovery rate, which was <1% for all identifications. In all cases, the fragmentation assignment was manually verified for all peptide spectra matches before assigning protein candidates.

2.4. Bioinformatic analysis

Functional annotation and network analysis were performed with STRING software (*http://string-db.org/*) and Cytoscape platform version 3.7.2 (*https://cytoscape.org*) using *Mus musculus* orthologous genes. In particular, the two plugins of Cytoscape, namely Cluego and Clupedia [34,35] were used to integrate the GO categories [Biological Process (BP), Molecular Function (MF), Cellular Component (CC)], Reactome Pathways, Kyoto Encyclopedia of Genes and Genomes (KEGG), and Wiki Pathways annotation. The κ score level was set at ≥0.4, while minimum and maximum levels were set at 3 and 8, respectively.

2.5. Western blotting

Immunoblotting analysis was performed to confirm the cell model characterization and for independent validation of DIGE results. Cells were lysed through incubation in TNE buffer (10 mM Tris-HCl pH 7.4, 150 mM NaCl, 5 mM EDTA and 0.5% v/v Triton X-100) containing protease and phosphatase cocktail inhibitors (Sigma-Aldrich), for 30 min, at 4 °C. Depending on the molecular mass of the component under evaluation, extracted proteins (30 μg of total material) were separated by 10% T or 12% T mini SDS-PAGE and blotted on PDVF membranes (Immun-Blot® PVDF Membrane, BioRad). Protein immunodetection was performed by incubating the membrane with primary antibodies against hamartin (1:1000, Cell Signaling), phospho-p70S6K(T389) (1:1000, Cell Signaling), p70S6K (1:1000, Cell Signaling), rabbit phospho-4E-BP1(T37/46) (1:1000, Cell Signaling), 4E-BP1 (1:1000, Cell Signaling), phospho-mTOR(S2448) (1:1000, Cell Signaling), mTOR (1:1000, Cell Signaling), cofilin 1 (CFL1) (Thermo Fisher Scientific, 1:2000), aldolase C (ALDOC) (Thermo Fisher Scientific, 1:2000), thioredoxin (TXN) (Thermo Fisher Scientific, 1:2000), beta-tubulin (Thermo Fisher Scientific, 1:8000) in 5% non-fat milk solutions of Tris-Buffered Saline (TBS), at 4 °C, overnight. Anti-rabbit HRP-conjugate antibody (Millipore, 1:10000) or anti-mouse HRP-conjugate (Millipore, 1:5000)

were used as secondary antibodies. Protein bands were visualized with Clarity Western ECL Substrate (Bio-Rad) and filtered images were acquired using a GS-800 imaging systems scanner (Bio-Rad). A densitometric analysis was performed with Quantity One 4.5.0 software (Bio-Rad) using tubulin as normalization factor. Western blot analyses for independent validation of DIGE results were performed using 3 different cell batches of $Tsc1^{ko}$ and $Tsc1^{wt}$. Data are expressed as mean ± SD (standard deviation); non-parametric unpaired *t*-test, two-tailed, with a 95% confidence interval was performed when 2 groups were compared using GraphPad Prism 5.0 software (GraphPad Software, Inc., San Diego, CA, USA). *P*-values below 0.05 were considered statistically significant.

3. Results

3.1. A murine CNS-derived cellular model of TSC

We here used murine postnatal SVZ $Tsc1^{wt}$ NSPCs to generate a *Tsc1*-deficient ($Tsc1^{ko}$) counterpart. This was done with the aim of having a cellular model of TSC disorder, which could be further investigated by proteomics to unveil the molecular mechanisms associated with the pathogenesis of this disease. To this purpose, $Tsc1^{ko}$ cells were generated and validated as reported in our previous study [3]. In particular, the activation of mTORC1 in $Tsc1^{ko}$ cells, with respect to $Tsc1^{wt}$ ones, was confirmed by measuring the corresponding increased phosphorylation levels of both p70S6K and 4E-BP1, which are known as molecular targets of mTORC1. Evident results were obtained in both cases (Fig. 1A). Activation of p70S6K was further confirmed by the increase in the phosphorylation (S235/236) levels of S6 ribosomal protein (Fig. 1B), which is known as a target of p70S6K. As expected, $Tsc1^{ko}$ cells also showed a proliferative rate higher than that of $Tsc1^{wt}$ cells (Fig. 1C). Further, the differentiation rate of $Tsc1^{ko}$ cells cultured in matrigel pre-coated wells and stimulated with both β-FGF2 and EGF for 24 h, appeared more pronounced compared to that of $Tsc1^{wt}$ cells. Abnormally enlarged nestin or GFAP-positive $Tsc1^{ko}$ cells were comparatively evidenced in the immunofluorescence images obtained by using

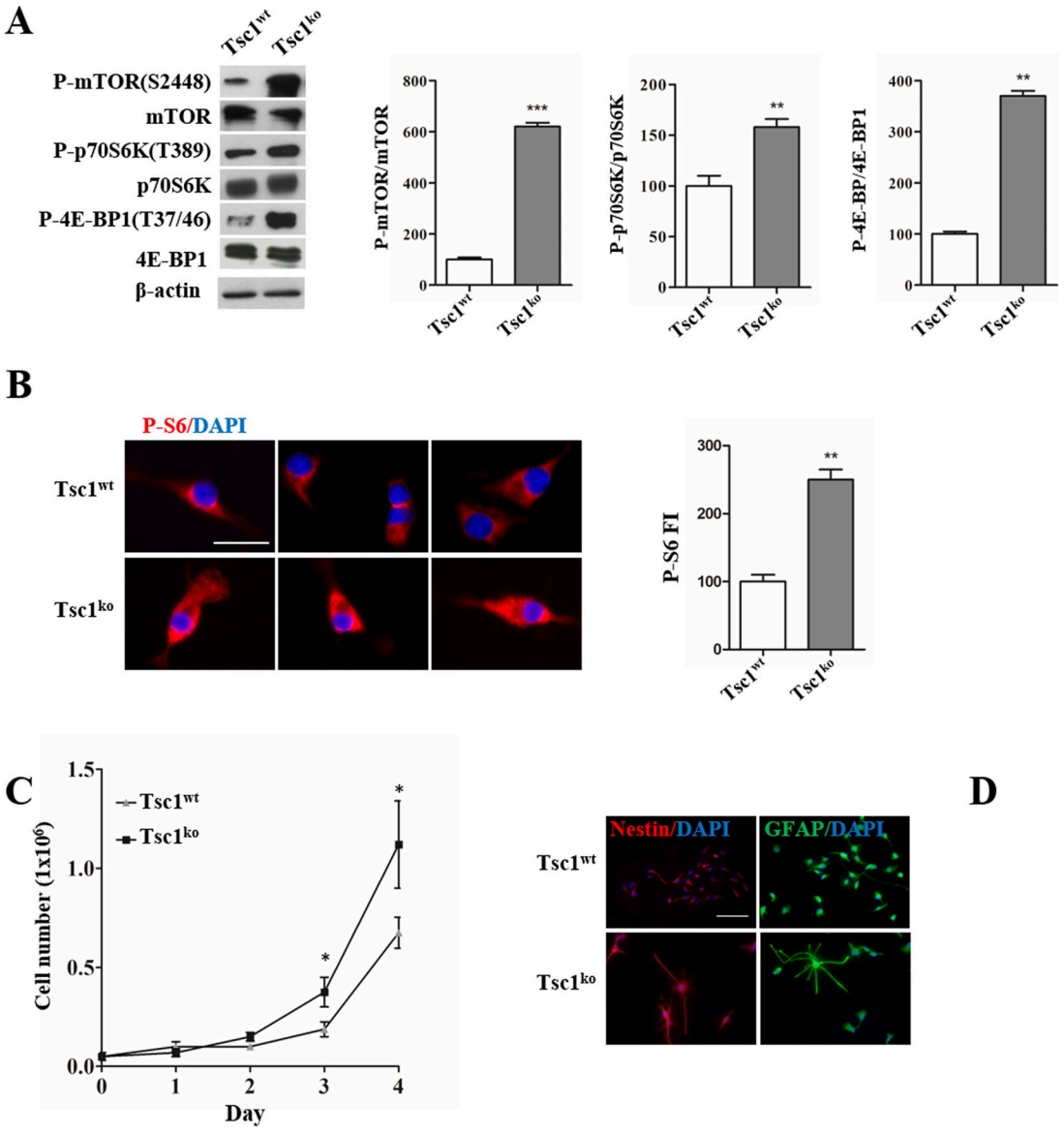

Fig. 1. A) Representative images and corresponding densitometric analyses of Western Blotting experiments; P-mTOR, Pp70S6K and P-4EBP1 were normalized over total mTOR, p70S6K and, 4E-BP1, respectively. Values are the mean ± SD of four independent experiments. ***$p < 0.001$, **$p < 0.01$ $Tsc1^{ko}$ vs $Tsc1^{wt}$. B) Immunofluorescence images (scale bar: 50 μm) of phospho-S6 ribosomal protein (S235/236) (P—S6) of NSPCs cultured in matrigel pre-coated glass coverslips, for 24 h. Bar graph of PS6-IF analysis, ***$p < 0.01$, $Tsc1^{ko}$ vs $Tsc1^{wt}$. C) Growth curve over 4 days. Values are the mean ± SD of four independent experiments. *$p < 0.05$ $Tsc1^{ko}$ vs $Tsc1^{wt}$. D) Immunofluorescence images of both nestin and GFAP of NSPCs cultured on matrigel pre-coated glass coverslips, for 24 h (scale bar: 100 μm).

antibodies against both neural stem cell protein markers (Fig. 1D).

3.2. Proteomic variations in Tsc1-deficient SVZ NSPCs

3.2.1. 2D-DIGE analysis

With the aim to define quantitative protein changes associated with different properties of $Tsc1^{ko}$ and $Tsc1^{wt}$ cells (Fig. 1), corresponding protein extracts were compared with the 2D-DIGE approach. In particular, $Tsc1^{ko}$ and $Tsc1^{wt}$ protein extracts were prepared as reported in the experimental section, labelled with specific dyes, resolved through two-dimensional electrophoresis and compared by dedicated analysis of corresponding gel images. A total of 1516 spots were matched over the gels, among which 55 ones resulted differentially represented ($p \leq 0.05$ and fold-change $\geq$1.5) in $Tsc1^{ko}$ versus $Tsc1^{wt}$ cell comparison. These spots are numbered and shown in a representative 2D-DIGE map (Fig. 2); they were selected for further protein identification, and thus picked and subjected to trypsinolysis, followed by nanoLC-ESI-Q-Orbitrap-MS/MS analysis. Identified proteins are listed in Table 1. Corresponding protein identification details are reported in Supplementary Table S1. Overall, 36 gene products were identified; among them 19 protein entries resulted over-represented in $Tsc1^{ko}$ cells, while 17 ones were down-represented therein. Some proteins were identified in multiple spots and always showed a coherent quantitative trend (Table 1).

3.2.2. Functional annotation

To highlight a possible functional relationship between differentially abundant proteins in $Tsc1^{ko}$ cells, identified components were subjected to analysis with Search Tool for the Retrieval of Interacting Genes (STRING). Various protein-protein interactions (PPIs) were detected, which depicted a unique network consisting of 36 nodes, 105 edges, 5.83 average node degree, 0.59 average local clustering coefficient and 24 expected edges (Fig. 3). The corresponding PPI enrichment *p*-value was 1.0 e^{-16}. A central core made of glyceraldehyde-3-phosphate dehydrogenase (Gapdh), fructose-bisphosphate aldolase A and C (AldoA and C), triosephosphate isomerase (Tpi1) and transaldolase (Taldo1) was detected in this network, also including various proteins related to redox stress, such as peroxiredoxin 6 (Prdx6), thioredoxin (Txn1) and glutathione S-transferase P1 (Gstp1).

The gene ontology (GO) analysis of the STRING output revealed that the most significant biological process (BP) categories were "response to oxidative stress", "response to reactive oxygen species", "response to nitrogen compound", "protein folding", and "carbohydrate metabolic process". Among cellular component (CC) assigned in the above-mentioned network, 13 proteins occur in myelin sheath; on the other hand, glycolysis and gluconeogenesis, oxidative stress and redox pathways were evidenced as enriched significant Wiki Pathways. The complete list of STRING annotations is reported in Supplementary Table S2.

A functional analysis was also performed by using two Cytoscape plugins, namely ClueGO and the CluePedia, and integrating GO terms and pathways such as biological processes, molecular functions, cellular component, reactome, KEGG annotations/genomes, and WikiPathways. The κ score level was set at $\geq$0.4. The main statistically significant ($p < 0.05$) functional groups annotating differentially abundant proteins in $Tsc1^{ko}$ cells were: i) oxidative stress and redox pathways; ii) methylglyoxal biosynthetic process; iii) regulation of synaptic transmission GABAergic; iv) myelin sheath; v) modification of post-synaptic actin cytoskeleton; vi) protein S-nitrosylation; vii) biochemical pathways related to carbohydrate metabolism; viii) dimethylarginase activity (Fig. 4).

3.2.3. Validation of proteomic results

Immunoblotting analyses were performed to validate differentially abundant proteins assigned after 2D-DIGE analysis of $Tsc1^{ko}$ versus $Tsc1^{wt}$ cell extracts. In particular, dedicated experiments were performed on aldolase, cofilin and thioredoxin (Fig. 5A and B); tubulin was used as housekeeping protein. These experiments confirmed the increase of all above-mentioned proteins, further supporting the hypothesized changes in glucose metabolism, cytoskeleton and oxidative stress in $Tsc1^{ko}$ cells, as measured by 2D-DIGE. Immunofluorescence images of

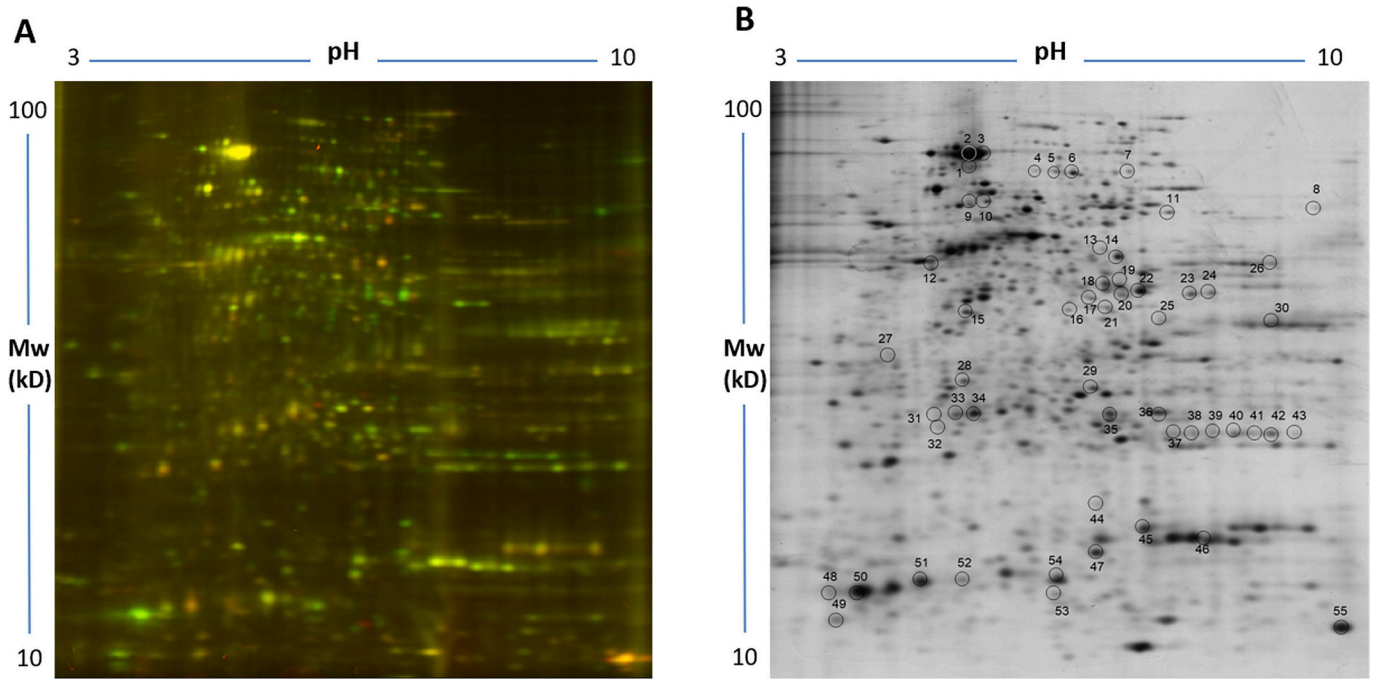

Fig. 2. Comparison of lysates from $Tsc1^{ko}$ and $Tsc1^{wt}$ cells. A) 2D-DIGE representative image of $Tsc1^{ko}$ sample (red, Cy3) vs. $Tsc1^{wt}$ sample (green, Cy5). Internal standard (pool, Cy2) is not shown. Overlapping spots in yellow. B) 2D representative image of the same gel post-stained with silver nitrate. Encircled and numbered spots resulted in consistently changed absorbance in the different sample groups; they were subjected to *in-gel* digestion with trypsin and were analyzed using nanoLC-ESI-Q-Orbitrap-MS/MS for protein identification. Spots with successful protein identification are reported in Table 1. (For interpretation of the references to colour in this figure legend, the reader is referred to the web version of this article.)

Table 1
Differentially represented protein spots in $Tsc1^{ko}$ versus $Tsc1^{wt}$ cells. Spot number (marked and numbered in Fig. 2), UniProtKB accession, protein accession, protein description, gene name, fold change value, corresponding *P* value, number of assigned unique peptides and Mascot score value are listed.

Spot n°	UniProtKB accession	Protein accession	Protein description	Gene name	AW ratio $Tsc1^{ko}$ vs $Tsc1^{wt}$	*P*-value	Unique peptides	Mascot score
1	P38647	GRP75_MOUSE	Stress-70 protein, mitochondrial	Hspa9	−1.60	0.025	10	595
2	Q8VBT9	ASPC1_MOUSE	Tether containing UBX domain for GLUT4	Aspscr1	−1.51	0.032	3	158
3	P80316	TCPE_MOUSE	T-complex protein 1 subunit epsilon	Cct5	−1.54	0.016	2	88
4	Q60864	STIP1_MOUSE	Stress-induced-phosphoprotein 1	Stip1	1.50	0.012	25	1339
5	Q60864	STIP1_MOUSE	Stress-induced-phosphoprotein 1	Stip1	1.60	0.00084	34	1826
6	Q60864	STIP1_MOUSE	Stress-induced-phosphoprotein 1	Stip1	1.85	0.000013	46	2600
7	Q8R081	HNRPL_MOUSE	Heterogeneous nuclear ribonucleoprotein L	Hnrnpl	1.61	0.017	18	990
8	Q9CY58	PAIRB_MOUSE	Plasminogen activator inhibitor 1 RNA-binding protein	Serbp1	3.41	0.000059	21	1114
9	P63038	CH60_MOUSE	60 kDa heat shock protein, mitochondrial	Hspd1	−1.88	5.3E-06	24	1439
10	P27773	PDIA3_MOUSE	Protein disulfide-isomerase A3	Pdia3	−1.76	0.0002	25	1314
11	Q91ZJ5	UGPA_MOUSE	UTP-glucose-1-phosphate uridylyltransferase	Ugp2	1.97	0.003	25	1334
12	P60710	ACTB_MOUSE	Actin, cytoplasmic 1	Actb	−1.61	0.00017	18	1120
13	P62196	PRS8_MOUSE	26 S proteasome regulatory subunit 8	Psmc5	−1.92	0.001	24	1036
14	O88844	IDHC_MOUSE	Isocitrate dehydrogenase [NADP] cytoplasmic	Idh1	−1.76	0.002	33	2026
15	Q9CWS0	DDAH1_MOUSE	N(G),N(G)-dimethylarginine dimethylaminohydrolase 1	Ddah1	−1.92	0.000053	11	580
16	P45376	ALDR_MOUSE	Aldose reductase	Akr1b1	1.61	0.0069	14	822
17	Q93092	TALDO_MOUSE	Transaldolase	Taldo1	−1.53	0.00011	16	805
18	P05063	ALDOC_MOUSE	Fructose-bisphosphate aldolase C	Aldoc	1.67	0.02	15	936
19	P05063	ALDOC_MOUSE	Fructose-bisphosphate aldolase C	Aldoc	2.26	0.0001	21	1376
20	P05063	ALDOC_MOUSE	Fructose-bisphosphate aldolase C	Aldoc	1.62	3.5E-06	18	1172
21	P05063	ALDOC_MOUSE	Fructose-bisphosphate aldolase C	Aldoc	2.30	0.0018	27	1841
22	P10107	ANXA1_MOUSE	Annexin A1	Anxa1	2.36	0.00035	16	773
23	P05064	ALDOA_MOUSE	Fructose-bisphosphate aldolase A	Aldoa	1.55	0.000044	19	996
24	P05064	ALDOA_MOUSE	Fructose-bisphosphate aldolase A	Aldoa	1.55	0.000096	21	1353
25	P16858	G3P_MOUSE	Glyceraldehyde-3-phosphate dehydrogenase	Gapdh	1.54	0.024	13	828
26	P05064	ALDOA_MOUSE	Fructose-bisphosphate aldolase A	Aldoa	1.66	0.0016	21	1383
27	Q9CPV4	GLOD4_MOUSE	Glyoxalase domain-containing protein 4	Glod4	−1.65	0.0013	16	963
28	P97371	PSME1_MOUSE	Proteasome activator complex subunit 1	Psme1	−1.88	0.017	17	991
29	P00920	CAH2_MOUSE	Carbonic anhydrase 2	Ca2	1.71	0.00084	12	751
30	P16858	G3P_MOUSE	Glyceraldehyde-3-phosphate dehydrogenase	Gapdh	1.54	0.0017	16	1065
31	O08709	PRDX6_MOUSE	Peroxiredoxin-6	Prdx6	−1.63	0.022	12	592
32	P61759	PFD3_MOUSE	Prefoldin subunit 3	Vbp1	−2.08	0.00063	12	674
33	O08709	PRDX6_MOUSE	Peroxiredoxin-6	Prdx6	−1.59	0.026	7	343
34	O08709	PRDX6_MOUSE	Peroxiredoxin-6	Prdx6	−1.60	0.038	26	1944
35	P17751	TPIS_MOUSE	Triosephosphate isomerase	Tpi1	1.77	0.0015	17	1268
36	P17751	TPIS_MOUSE	Triosephosphate isomerase	Tpi1	1.96	0.0011	17	1319
37	P19157	GSTP1_MOUSE	Glutathione S-transferase P 1	Gstp1	1.59	0.0047	9	649
38	P19157	GSTP1_MOUSE	Glutathione S-transferase P 1	Gstp1	2.19	0.0028	12	935
39	P19157	GSTP1_MOUSE	Glutathione S-transferase P 1	Gstp1	1.79	0.000071	13	1007
40	P19157	GSTP1_MOUSE	Glutathione S-transferase P 1	Gstp1	2.76	7.2E-08	9	639
41	P19157	GSTP1_MOUSE	Glutathione S-transferase P 1	Gstp1	3.26	1.8E-06	13	962
42	P19157	GSTP1_MOUSE	Glutathione S-transferase P 1	Gstp1	2.72	3E-07	8	617
43	P19157	GSTP1_MOUSE	Glutathione S-transferase P 1	Gstp1	2.05	0.00063	11	840
44	Q01768	NDKB_MOUSE	Nucleoside diphosphate kinase B	Nme2	−1.63	0.0036	6	323
45	P18760	COF1_MOUSE	Cofilin-1	Cfl1	1.75	0.0071	13	699
46	P17742	PPIA_MOUSE	Peptidyl-prolyl *cis-trans* isomerase A	Ppia1	1.53	0.00031	12	898
47	P15532	NDKA_MOUSE	Nucleoside diphosphate kinase A	Nme1	1.55	0.0012	9	584
48	P10639	THIO_MOUSE	Thioredoxin	Txn	2.27	0.000089	6	318
49	P62077	TIM8B_MOUSE	Mitochondrial import inner membrane translocase subunit Tim8 B	Timm8b	1.65	0.0087	4	248
50	P10639	THIO_MOUSE	Thioredoxin	Txn	2.97	0.000062	9	471
51	P51880	FABP7_MOUSE	Fatty acid-binding protein, brain	Fabp7	−1.89	8.8E-06	9	559
52	P51880	FABP7_MOUSE	Fatty acid-binding protein, brain	Fabp7	−1.74	0.000033	10	632
53	P62962	PROF1_MOUSE	Profilin-1	Pfn1	1.51	0.0013	8	492
54	P70349	HINT1_MOUSE	Histidine triad nucleotide-binding protein	Hint1	1.85	0.00013	9	499
55	P31786	ACBP_MOUSE	Acyl-CoA-binding protein	Dbi	−2.06	0.00047	10	631

cells stained with fluorescent-labelled phalloidin further confirmed the occurrence of cytoskeletal changes in $Tsc1^{ko}$ cells compared to $Tsc1^{wt}$ ones (Fig. 5C), as already hypothesized by proteomics.

4. Discussion

The aim of this study was to carry out a proteomic investigation of a cellular model of TSC. The investigated disease may be based on mutations of either of two genes, *Tsc1* and *Tsc2*, whose protein products, hamartin and tuberin, form a functional signaling complex. The mutations affect the interaction of hamartin and tuberin, inactivating their complex and thus the downstream cellular signaling pathways. Both gene mutations are reported to create similar pathogenesis [11]. Our model was already obtained earlier and characterized as deriving from murine postnatal SVZ NSPCs after deletion of the *Tsc1* gene, described in our previous paper [3]. Resulting $Tsc1^{ko}$ cells exhibited similar characteristics to TSC neural cells, such as hyperactivation of the mTORC1 signaling pathway, which result in an abnormally enlarged astrocyte-like cell formation, increased cell proliferation rate and altered cell migration pattern. Moreover, autophagy dysfunction and reduced

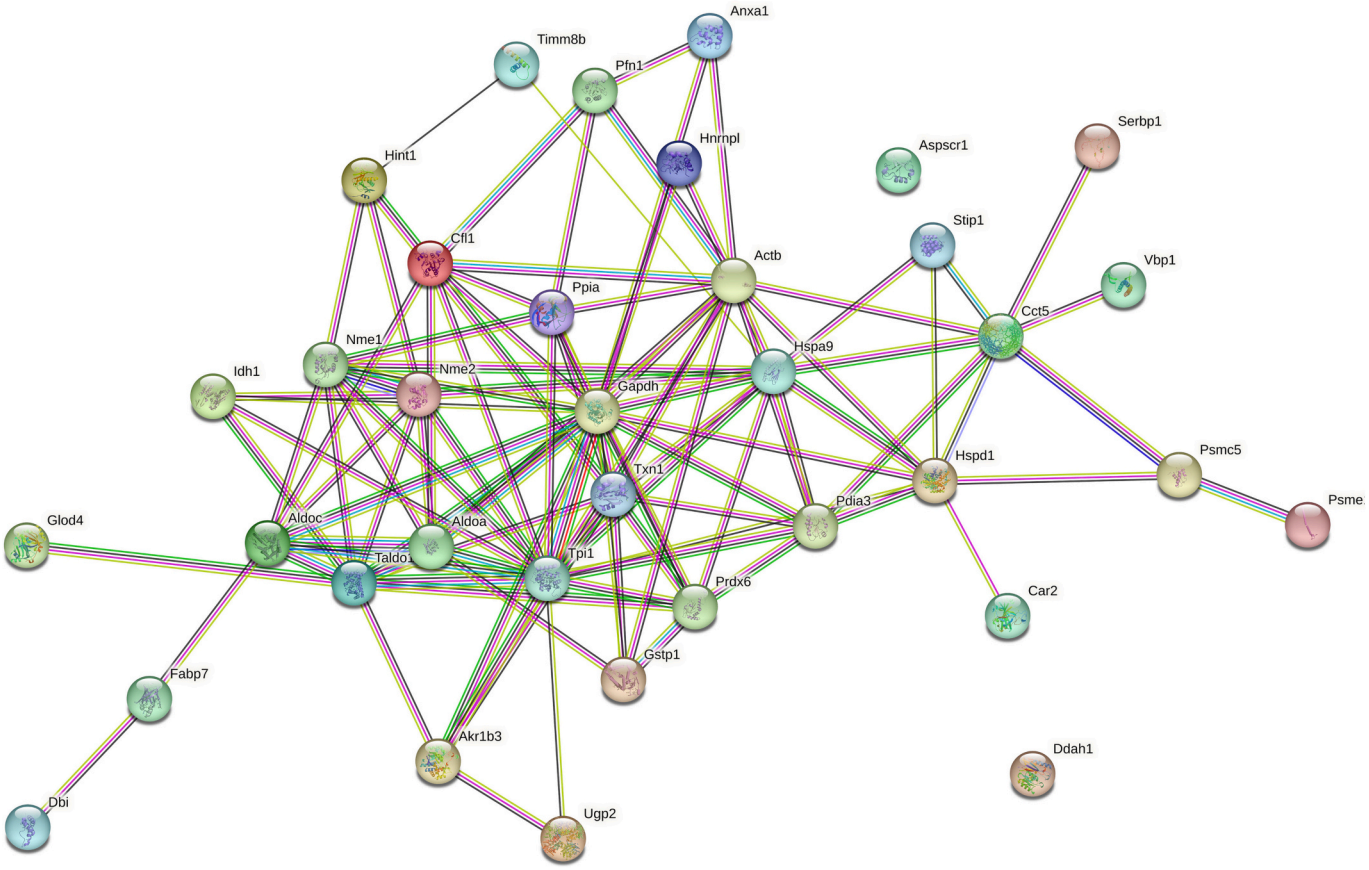

Fig. 3. Protein-protein interaction (PPI) of differentially abundant proteins in $Tsc1^{ko}$ versus $Tsc1^{wt}$ cells (PPI enrichment *p*-value: $<1.0^{e-16}$) after STRING analysis. Functional protein association network of proteins listed in Table 1, as deriving from a database search in STRING. Gene name of proteins are reported, for full names see Table 1.

nuclear TFEB levels were also observed. Some of these characteristics were preliminary tested in this study to confirm the observed properties of this cellular model of disorder and to correlate them with proteomic results. Overall, proteomic results revealed some differentially represented proteins that highlighted peculiar molecular differences between $Tsc1^{ko}$ and $Tsc1^{wt}$ cells, indirectly suggesting putative biochemical pathways involved in the pathogenesis of TSC-associated disorders.

Proteomic results revealed alterations in cytoskeletal proteins that may explain the changes in cell morphology and dendritic spine structure already reported in TSC cells, which were previously observed in $Tsc1^{ko}$ cells as well and confirmed here. Functional analysis of differentially represented proteins in $Tsc1^{ko}$ cells highlighted the term "modification of postsynaptic actin cytoskeleton". In particular, elevated levels of profilin 1 and cofilin were observed in $Tsc1^{ko}$ cells. These important actin-binding proteins control actin polymerization, dynamics and function [36]. Moreover, profilin 1 plays a crucial role in extra-synaptic functions and is required in brain morphogenesis for the maintenance of the neuronal stem-cell compartment and the generation of the differentiated neurons [37]. This protein is also involved in the pathogenesis of neurological disorders, such as amyotrophic lateral sclerosis and Fragile X syndrome [38], and acts as both an oncogenic and tumor suppressor in cancer cells [38]. Cofilin is an actin depolymerising factor that has already been associated with cytoskeleton and morphological changes of TSC cells [39]. In the context of cell cytoskeleton, worth mentioning was also the observed down-representation in $Tsc1^{ko}$ cells of T-complex protein 1 subunit epsilon (CCT5) and prefoldin, which are both essential components of the protein quality control machinery and chaperones involved in the co-translational folding of cytoskeletal proteins. CCT5 is a component of the TRiC/CCT complex, which is essential for cellular protein folding [40], while prefoldin acts as a co-chaperone that transfers cytoskeletal proteins to TRiC/CCT [41]. Indeed, CCT5 depletion was demonstrated to induce uncontrolled proliferation, altered dendrite morphogenesis and retarded dendrite growth in neurons [42], as already observed in TSC.

GO analysis of differentially represented proteins in $Tsc1^{ko}$ cells also highlighted that further structural changes probably occur in the "myelin sheath", as already observed in the frontal cortex and hippocampus of *Tsc1*-deficient mice [28]. Interestingly, $Tsc1^{ko}$ cells showed a down-representation of fatty acid-binding protein 7 (FABP7), which is one of the factors affecting disorganized axonal myelinogenesis, a well-known feature of TSC neurological disorders. Indeed, FABP7 is the main fatty acid binding protein found in astrocytes/oligodendrocytes, and plays a pivotal role in developmental myelination and myelin sheath formation [43,44]. Moreover, the observed decreased levels of FABP7 in $Tsc1^{ko}$ cells suggested a possible impact of this protein on cell migration [3], as depletion of this protein in FABP7-expressing astrocytes resulted in a reduction of this phenomenon [43].

Further, $Tsc1^{ko}$ cells showed increased levels of heterogeneous nuclear ribonucleoprotein L (hnRNPL) [45], UTP-glucose-1-phosphate uridylyltransferase (UGP2) [46] and nucleoside diphosphate kinase A (NME1). The increase of these proteins in $Tsc1^{ko}$ cells could explain the alterations of cellular proliferation, differentiation and migration that were previously observed in this model of TSC disease [3], and were further confirmed in this study. In particular, hnRNPL is an RNA binding protein that is highly expressed in *TSC1*- and *TSC2*-deficient cells [47]. NME1 plays an important role in the synthesis of nucleoside triphosphates and Ser/Thr phosphorylation; this protein was already found over-represented in mouse models of mTOR-driven hepatocellular

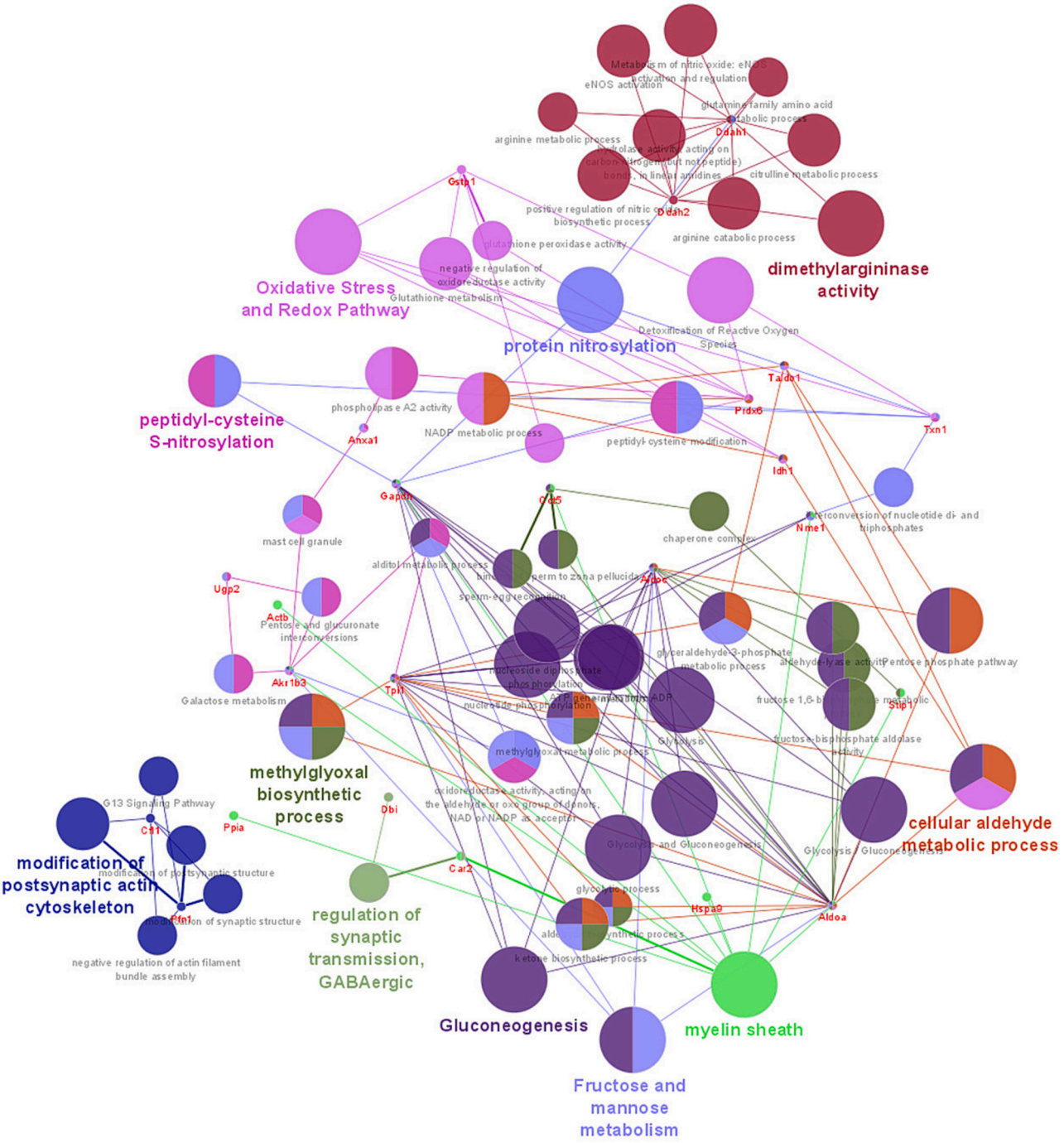

Fig. 4. ClueGO network of differentially abundant proteins in Tsc1^{ko} versus Tsc1^{wt} cells. Functional analysis was performed by integrating Ontologies and Pathways including Biological Process, Molecular Function, Cellular Component, Reactome, KEGG, and WikiPathway output.

carcinoma [48].

Differentially abundant proteins in Tsc1^{ko} cells also included components involved in "regulation of synaptic transmission GABAergic" and "methylglyoxal (MG) biosynthetic process", thus supporting the notion that synaptic functions as well as neurotransmitter systems might also be affected in TSC disease. The alteration of the GABAergic transmission system has already been described in *TSC*-deficient cells and TSC neurological disorders, such autism spectrum disorders (ASD) and epilepsy [49]; conversely, the impairment the MG system has never been related to TSC so far. Interestingly, the reduction in the glyoxalase domain-containing protein 4 (iso4) observed in Tsc1^{ko} cells may be hypothetically associated with a corresponding, hypothetical increase of MG therein. GLOD4 is a member of the glyoxalase 1 (GLO1) family and belongs to the glyoxalase system, which catalyses the detoxification of the methylglyoxal into D-lactate. The effects of MG seem to be mediated by GABA receptors, as it is classified as a GABA agonist [50]. Moreover, MG is a highly reactive compound that can react with proteins forming advanced glycation end-products (AGEs) [51]. MG accumulation in the brain plays a role in the pathogenesis of autism, whereas high MG and AGEs levels have already been associated with protein misfolding, oxidative stress, and glutamate system disturbance [51]. In this context, Yang and colleagues demonstrated that a reduction of GLO1 levels in embryonic mouse cortical neural precursor cells induces premature neurogenesis and long-term alterations in cortical neurons postnatally

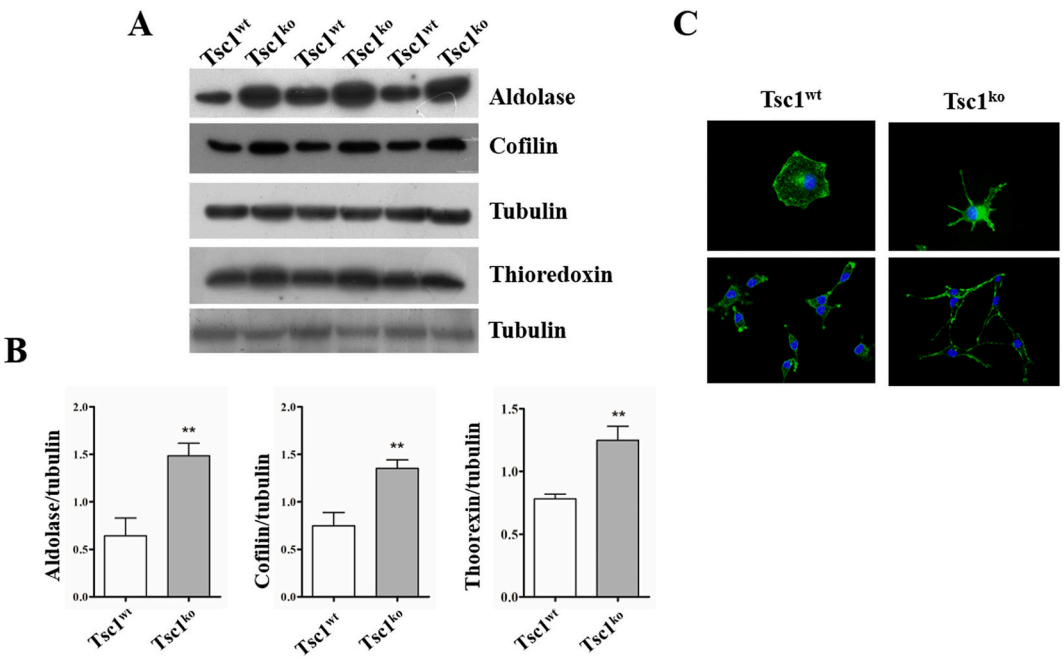

Fig. 5. Validation of proteomic results. A) Representative images of Western blotting experiments obtained using Ab against aldolase, cofilin, thioredoxin and tubulin; the latter was used as housekeeping protein. B) Bar graphs of results reported in panel A. Data represent the mean ± SD. *$p < 0.05$ $Tsc1^{ko}$ versus $Tsc1^{wt}$ cells of three independent blots. C) Actin cytoskeleton analysis by fluorescent phalloidin, scale bar = 50 μm.

[52]. An impairment of the glyoxalase system however has never been linked to TSC-related diseases. On the other hand, MG is a deviation product of glycolysis that - as expected - may be upregulated in $Tsc1^{ko}$ cells, as we found an increased representation of glycolytic enzymes (GAPDH, ALDOA, ALDOC and TPI1). Upregulation of carbohydrate metabolism has already been described in TSC-related disorders [53,54], and glycolytic inhibitors have been previously proposed as therapeutic agents for the treatment of TSC-associated tumors [55,56]. Notably, our results strengthen the idea that an alteration of glucose metabolism generally occur in TSC cells. Overall, our proteomic data on the activation of the glycolytic pathways in $Tsc1^{ko}$ cells are also in good agreement with the corresponding cell medium acidification already described by our previous paper [3]. However, concomitant mechanisms can contribute this phenomenon in $Tsc1^{ko}$ cells, such as those involving the increased representation of carbonic anhydrase (CA) II, as reported in this study. Cytosolic CA II is widely present in various cancers, including brain tumors and in other TSC mouse models [57]. CAs can help to stabilize intracellular pH of tumor cells as well as extracellular acidification associated with high metabolic rates and the malignant behaviour of cancer cells [57,58].

Differentially abundant proteins in $Tsc1^{ko}$ cells also included components involved in “oxidative stress and redox pathways”. This is not surprising since high levels of reactive oxygen species (ROS) and oxidative stress have already been described in TSC-deficient neurons [59], and a correlation between redox balance and mTORC1 signaling was previously established [60]. However, our results also move attention toward nitrosative stress, as protein S-nitrosylation was one of the terms evidenced in our functional analysis of deregulated components in $Tsc1^{ko}$ cells. Indeed, altered levels of peroxiredoxin 6, glutathione S-transferase P1 and thioredoxin were observed in these cells. In addition to exert an antioxidative function, these components act in glutathione and redoxin systems modulating S-nitrosylation/S-denitrosylation of proteins [61]. By possibly altering protein conformation, this post-translational modification was already described playing a crucial role for neuronal differentiation and maturation [62]; recently, it was also reported as a cause of cancer and neurodegenerative diseases, as well as autism spectrum disorders [63]. In agreement with results of this study, glutathione- and thioredoxin-dependent pathways were already proposed as promising therapeutic targets for TSC-associated tumors [64]. The occurrence of oxidative/nitrosative stress in $Tsc1^{ko}$ cells was also suggested by the observed reduced levels of NADP+-dependent isocitrate dehydrogenase (IDH1) and N(G),N(G)-dimethylarginine dimethylaminohydrolase (DDAH1). In this context, IDH1 is a cytoplasmic source of NADPH, which plays a key role in the cellular defence against oxidative stress [65], while DDAH1 acts in maintaining homeostatic control of NO by interacting with the nitric oxide synthases (NOSs). A further suggestion of the impairment of antioxidant pathways in $Tsc1^{ko}$ cells was the corresponding low abundance of cyclophilin A (CyP-A) [66]. This protein is abundant in brain tissues [67] and is secreted into the extracellular environment in response to oxidative stress [68]. In the brain, CyP-A seems to sustain antioxidant defences by modulating selenium transport [68].

Finally, proteomic analysis of $Tsc1^{ko}$ cells also suggested an impairment of the proteasome systems, as decreased levels of proteasome activator complex subunit 1 (PSME1) and 26S proteasome regulatory subunit 8 (PSMC5) were observed. In this context, there is still much debate regarding the role of mTOR signaling in proteasome-mediated protein degradation. In particular, Zhang and colleagues suggested that mTOR signaling increases the proteasome-mediated degradation of proteins with the final goal to supply building blocks to stimulate biosynthesis of novel polypeptide molecules [69]. Conversely, Zhao and co-workers [70] reported that mTOR activation inhibits both autophagy and proteasomal degradation. In agreement with the latter observation, Rousseau and Bertolotti reported that mTOR activation induces a decrease in proteasome abundance [71], which is rapidly alleviated upon TORC1 inhibition. Additional information on deregulated protein biosynthetic pathways in $Tsc1^{ko}$ cells were deduced from corresponding high levels of plasminogen activator inhibitor 1 RNA-binding protein (SERBP1). This protein was already reported modulating mRNA stability and protein synthesis, and was already linked to the development of numerous tumor types and neurogenesis [72–74].

5. Conclusion

In the present study, a comparative proteomic analysis of murine neuronal $Tsc1^{ko}$ and $Tsc1^{wt}$ cells has been performed. Results evidenced changes in the relative abundance of 36 proteins, which have been annotated in different cellular pathways. Some of these pathways have already been linked to TSC features, confirming the validity of this cellular model of TSC disorder. Novel protein players were also highlighted that in a next future may possibly contribute to clarify the molecular processes underling TSC pathophysiology, which is still poorly understood. In particular, we evidenced changes in proteins involved in cytoskeleton remodelling, glucose metabolism, oxidative/nitrosative stress, methylglyoxal biosynthesis, synaptic function, neurotransmitter systems as well as in neurogenesis. Some of proteins have never been associated with TSC-related disorders. However, the various pathogenic variants of *Tsc1* and *Tsc2* genes and the high variability of TSC clinical manifestations require different approaches and models of investigation. The impaired cellular pathways evidenced in our study could be investigated in other TSC models as they might represent, in the next future, potential pharmacological targets of TSC for innovative therapeutic strategies.

CRediT authorship contribution statement

Elisabetta Chiaradia: Conceptualization, Methodology, Data curation, Visualization, Writing – original draft. **Ingrid Miller:** Methodology, Investigation, Data curation, Supervision. **Giovanni Renzone:** Investigation, Data curation. **Alessia Tognoloni:** Investigation, Data curation. **Alice Polchi:** Investigation. **Federico De Marco:** Investigation. **Brunella Tancini:** Conceptualization, Writing – original draft. **Andrea Scaloni:** Conceptualization, Methodology, Supervision. **Alessandro Magini:** Conceptualization, Methodology, Investigation, Data curation, Funding acquisition.

Declaration of Competing Interest

The authors declare no competing financial interest.

Data availability

No

Acknowledgements

This work was supported by Associazione Sclerosi Tuberosa - Fondazione Terzo Pilastro-Italia e Mediterraneo (Project “ISDIS- Innovazione Scientifica e Disseminazione Sociale per la cura dei tumori cerebrali nella Sclerosi Tuberosa Complessa), Rome, Italy. E.C. and I.M. would like to acknowledge the Erasmus + STT mobility program (SS18) which enabled performing practical experiments together and exchange of knowledge.

Appendix A. Supplementary data

Supplementary data to this article can be found online at https://doi.org/10.1016/j.jprot.2023.104928.

References

[1] D. Alsowat, R. Whitney, S. Hewson, P. Jain, V. Chan, N. Kabir, K. Amburgey, D. Noone, M. Lemaire, B. McCoy, M. Zak, The phenotypic Spectrum of tuberous sclerosis complex: A Canadian cohort, Child. Neurol. Open 8 (2021), https://doi.org/10.1177/2329048X211012817, 2329048X2110128.
[2] P. Curatolo, R. Bombardieri, S. Jozwiak, Tuberous sclerosis, Lancet. 372 (2008) 657–668, https://doi.org/10.1016/S0140-6736(08)61279-9.
[3] A. Magini, A. Polchi, D. di Meo, G. Mariucci, K. Sagini, F. de Marco, T. Cassano, S. Giovagnoli, D. Dolcetta, C. Emiliani, TFEB activation restores migration ability to Tsc1-deficient adult neural stem/progenitor cells, Hum. Mol. Genet. 26 (2017) 3303–3312, https://doi.org/10.1093/HMG/DDX214.
[4] A. Polchi, A. Magini, D. di Meo, B. Tancini, C. Emiliani, mTOR Signaling and Neural Stem Cells: The Tuberous Sclerosis Complex Model, Int. J. Mol. Sci. 19 (2018) 1474, 10.3390/ijms19051474.202310.3390/ijms19051474.
[5] A.R. Tee, J.R. Sampson, D.K. Pal, J.M. Bateman, The role of mTOR signalling in neurogenesis, insights from tuberous sclerosis complex, Semin. Cell Dev. Biol. 52 (2016) 12–20, https://doi.org/10.1016/J.SEMCDB.2016.01.040.
[6] A.M. Heberle, U. Rehbein, M.R. Peiris, K. Thedieck, Finding new edges: systems approaches to MTOR signaling, Biochem. Soc. Trans. 49 (2021) 41–54, https://doi.org/10.1042/BST20190730.
[7] D.M. Sabatini, Twenty-five years of mTOR: uncovering the link from nutrients to growth, Proc. Natl. Acad. Sci. U. S. A. 114 (2017) 11818–11825, https://doi.org/10.1073/PNAS.1716173114.
[8] G.Y. Liu, D.M. Sabatini, mTOR at the nexus of nutrition, growth, ageing and disease, Nat. Rev. Mol. Cell Biol. 21 (2020) 183–203, https://doi.org/10.1038/S41580-019-0199-Y.
[9] A.-S. de Meulemeester, L. Heylen, A. Siekierska, J.D. Mills, A. Romagnolo, N.N. van der Wel, E. Aronica, P.A.M. de Witte, Hyperactivation of mTORC1 in a double hit mutant zebrafish model of tuberous sclerosis complex causes increased seizure susceptibility and neurodevelopmental abnormalities, Front. Cell Dev. Biol. 10 (2022), https://doi.org/10.3389/FCELL.2022.952832.
[10] P.B. Crino, K.L. Nathanson, E.P. Henske, The tuberous sclerosis complex, N. Engl. J. Med. 355 (2006) 1345–1356, https://doi.org/10.1056/NEJMRA055323.
[11] C.L. Salussolia, K. Klonowska, D.J. Kwiatkowski, M. Sahin, Genetic etiologies, diagnosis, and treatment of tuberous sclerosis complex, Annu. Rev. Genomics Hum. Genet. 20 (2019) 217–240, https://doi.org/10.1146/ANNUREV-GENOM-083118-015354.
[12] K.A. Orlova, P.B. Crino, The tuberous sclerosis complex, Ann. N. Y. Acad. Sci. 1184 (2010) 87–105, https://doi.org/10.1111/J.1749-6632.2009.05117.X.
[13] K.C. Ess, C.A. Kamp, B.P. Tu, D.H. Gutmann, Developmental origin of subependymal giant cell astrocytoma in tuberous sclerosis complex, Neurology. 64 (2005) 1446–1449, https://doi.org/10.1212/01.WNL.0000158653.81008.49.
[14] C.W. Shepherd, M.R. Gomez, J.T. Lie, C.S. Crowson, Causes of death in patients with tuberous sclerosis, Mayo Clin. Proc. 66 (1991) 792–796, https://doi.org/10.1016/S0025-6196(12)61196-3.
[15] L. Magri, M. Cominelli, M. Cambiaghi, M. Cursi, L. Leocani, F. Minicucci, P. L. Poliani, R. Galli, Timing of mTOR activation affects tuberous sclerosis complex neuropathology in mouse models, Dis. Model. Mech. 6 (2013) 1185–1197, https://doi.org/10.1242/DMM.012096.
[16] J. Zhou, G. Shrikhande, J. Xu, R.M. Mckay, D.K. Burns, J.E. Johnson, L.F. Parada, Tsc1 mutant neural stem/progenitor cells exhibit migration deficits and give rise to subependymal lesions in the lateral ventricle, Genes Dev. 25 (2011) 1595–1600, https://doi.org/10.1101/GAD.16750211.
[17] L. Magri, M. Cambiaghi, M. Cominelli, C. Alfaro-Cervello, M. Cursi, M. Pala, A. Bulfone, J.M. Garca-Verdugo, L. Leocani, F. Minicucci, P.L. Poliani, R. Galli, Sustained activation of mTOR pathway in embryonic neural stem cells leads to development of tuberous sclerosis complex-associated lesions, Cell Stem Cell 9 (2011) 447–462, https://doi.org/10.1016/J.STEM.2011.09.008.
[18] P.B. Crino, Evolving neurobiology of tuberous sclerosis complex, Acta Neuropathol. 125 (2013) 317–332, https://doi.org/10.1007/S00401-013-1085-X.
[19] J.D. Blair, H.S. Bateup, New frontiers in modeling tuberous sclerosis with human stem cell-derived neurons and brain organoids, Dev. Dyn. 249 (2020) 46–55, https://doi.org/10.1002/DVDY.60.
[20] K. Switon, K. Kotulska, A. Janusz-Kaminska, J. Zmorzynska, J. Jaworski, Molecular neurobiology of mTOR, Neuroscience. 341 (2017) 112–153, https://doi.org/10.1016/J.NEUROSCIENCE.2016.11.017.
[21] N.W. Hartman, T.V. Lin, L. Zhang, G.E. Paquelet, D.M. Feliciano, A. Bordey, mTORC1 targets the translational repressor 4E-BP2, but not S6 kinase 1/2, to regulate neural stem cell self-renewal in vivo, Cell Rep. 5 (2013) 433–444, https://doi.org/10.1016/J.CELREP.2013.09.017.
[22] D.M. Feliciano, J.L. Quon, T. Su, M.M. Taylor, A. Bordey, Postnatal neurogenesis generates heterotopias, olfactory micronodules and cortical infiltration following single-cell Tsc1 deletion, Hum. Mol. Genet. 21 (2012) 799–810, https://doi.org/10.1093/HMG/DDR511.
[23] D.M. Feliciano, T. Su, J. Lopez, J.C. Platel, A. Bordey, Single-cell Tsc1 knockout during corticogenesis generates tuber-like lesions and reduces seizure threshold in mice, J. Clin. Invest. 121 (2011) 1596–1607, https://doi.org/10.1172/JCI44909.
[24] C.A. Lafourcade, T.V. Lin, D.M. Feliciano, L. Zhang, L.S. Hsieh, A. Bordey, Rheb activation in subventricular zone progenitors leads to heterotopia, ectopic neuronal differentiation, and rapamycin-sensitive olfactory micronodules and dendrite hypertrophy of newborn neurons, J. Neurosci. 33 (2013) 2419–2431, https://doi.org/10.1523/JNEUROSCI.1840-12.2013.
[25] C. Luo, W.R. Ye, W. Shi, P. Yin, C. Chen, Y.B. He, M.F. Chen, X. Bin Zu, Y. Cai, Perfect match: mTOR inhibitors and tuberous sclerosis complex, Orphanet. J. Rare. Dis. 17 (2022), https://doi.org/10.1186/S13023-022-02266-0.
[26] M. Nabavi Nouri, M. Zak, P. Jain, R. Whitney, Epilepsy Management in Tuberous Sclerosis Complex: existing and evolving therapies and future considerations, Pediatr. Neurol. 126 (2022) 11–19, https://doi.org/10.1016/J.PEDIATRNEUROL.2021.09.017.
[27] Y.D. Liu, M.Y. Ma, X. Bin Hu, H. Yan, Y.K. Zhang, H.X. Yang, J.H. Feng, L. Wang, H. Zhang, B. Zhang, Q.B. Li, J.C. Zhang, Q.X. Kong, Brain proteomic profiling in intractable epilepsy caused by TSC1 truncating mutations: A small sample study, Front. Neurol. 11 (2020), https://doi.org/10.3389/FNEUR.2020.00475.

[28] H. Wesseling, Y. Elgersma, S. Bahn, A brain proteomic investigation of rapamycin effects in the Tsc1+/− mouse model, Mol. Autism. 8 (2017), https://doi.org/10.1186/S13229-017-0151-Y.
[29] J. Shin, M. Kim, H.J. Jung, H.L. Cha, H. Suh-Kim, S. Ahn, J. Jung, Y.A. Kim, Y. Jun, S. Lee, D. Hwang, J. Kim, Characterization of developmental defects in the forebrain resulting from hyperactivated mTOR signaling by integrative analysis of transcriptomic and proteomic data, Sci. Rep. 7 (2017), https://doi.org/10.1038/S41598-017-02842-6.
[30] M.M. Bradford, A rapid and sensitive method for the quantitation of microgram quantities of protein utilizing the principle of protein-dye binding, Anal. Biochem. 72 (1976) 248–254, https://doi.org/10.1006/ABIO.1976.9999.
[31] I. Miller, Application of 2D DIGE in animal proteomics, Methods Mol. Biol. 854 (2012) 373–396, https://doi.org/10.1007/978-1-61779-573-2_26.
[32] L. Cesaratto, C. Vascotto, C. D'Ambrosio, A. Scaloni, U. Baccarani, I. Paron, G. Damante, S. Calligaris, F. Quadrifoglio, C. Tiribelli, G. Tell, Overoxidation of peroxiredoxins as an immediate and sensitive marker of oxidative stress in HepG2 cells and its application to the redox effects induced by ischemia/reperfusion in human liver, Free Radic. Res. 39 (2005) 255–268, https://doi.org/10.1080/10715760400029603.
[33] J. Zhu, S. Arena, S. Spinelli, D. Liu, G. Zhang, R. Wei, C. Cambillau, A. Scaloni, G. Wang, P. Pelosi, Reverse chemical ecology: olfactory proteins from the giant panda and their interactions with putative pheromones and bamboo volatiles, Proc. Natl. Acad. Sci. U. S. A. 114 (2017) E9802–E9810, https://doi.org/10.1073/PNAS.1711437114.
[34] G. Bindea, B. Mlecnik, H. Hackl, P. Charoentong, M. Tosolini, A. Kirilovsky, W. H. Fridman, F. Pagès, Z. Trajanoski, J. Galon, ClueGO: A Cytoscape plug-in to decipher functionally grouped gene ontology and pathway annotation networks, Bioinformatics. 25 (2009) 1091–1093, https://doi.org/10.1093/bioinformatics/btp101.
[35] G. Bindea, J. Galon, B. Mlecnik, CluePedia Cytoscape plugin: pathway insights using integrated experimental and in silico data, Bioinformatics. 29 (2013) 661–663, https://doi.org/10.1093/bioinformatics/btt019.
[36] W. Lehman, Y. Maéda, Introducing a special issue of the journal of muscle research and cell motility on actin and actin-binding proteins, J. Muscle Res. Cell Motil. 41 (2020), https://doi.org/10.1007/S10974-019-09569-Z.
[37] M. di Domenico, M. Jokwitz, W. Witke, P.P. Boyl, Specificity and redundancy of profilin 1 and 2 function in brain development and neuronal structure, Cells. 10 (2021), https://doi.org/10.3390/CELLS10092310.
[38] K. Murk, M. Ornaghi, J. Schiweck, Profilin isoforms in health and disease – all the same but different, Front. Cell Dev. Biol. 9 (2021) 2086, https://doi.org/10.3389/FCELL.2021.681122/BIBTEX.
[39] S.F. Tavazoie, V.A. Alvarez, D.A. Ridenour, D.J. Kwiatkowski, B.L. Sabatini, Regulation of neuronal morphology and function by the tumor suppressors Tsc1 and Tsc2, Nat. Neurosci. 12 (8) (2005) 1727–1734, https://doi.org/10.1038/nn1566.
[40] I. Tahmaz, S. Shahmoradi Ghahe, U. Topf, Prefoldin function in cellular protein homeostasis and human diseases., front cell, Dev. Biol. 9 (2021), 816214, https://doi.org/10.3389/fcell.2021.816214.
[41] M.P. Collier, K.B. Moreira, K.H. Li, Y.C. Chen, D. Itzhak, R. Samant, A. Leitner, A. Burlingame, J. Frydman, Native mass spectrometry analyses of chaperonin complex TRiC/CCT reveal subunit N-terminal processing and re-association patterns, Sci. Rep. 11 (2021), https://doi.org/10.1038/S41598-021-91086-6.
[42] Y.H. Wang, Z.Y. Ding, Y.J. Cheng, C.T. Chien, M.L. Huang, An efficient screen for cell-intrinsic factors identifies the chaperonin CCT and multiple conserved mechanisms as mediating dendrite morphogenesis, Front. Cell. Neurosci. 14 (2020), https://doi.org/10.3389/FNCEL.2020.577315.
[43] M. Kipp, T. Clarner, S. Gingele, F. Pott, S. Amor, P. van der Valk, C. Beyer, Brain lipid binding protein (FABP7) as modulator of astrocyte function, Physiol. Res. 60 (2011), https://doi.org/10.33549/PHYSIOLRES.932168.
[44] E. Ercan, J.M. Han, A. di Nardo, K. Winden, M.J. Han, L. Hoyo, A. Saffari, A. Leask, D.H. Geschwind, M. Sahin, Neuronal CTGF/CCN2 negatively regulates myelination in a mouse model of tuberous sclerosis complex, J. Exp. Med. 214 (2017) 681–697, https://doi.org/10.1084/JEM.20160446.
[45] J. Gu, Z. Chen, X. Chen, Z. Wang, Heterogeneous nuclear ribonucleoprotein (hnRNPL) in cancer, Clin. Chim. Acta 507 (2020) 286–294, https://doi.org/10.1016/J.CCA.2020.04.040.
[46] A.L. Wolfe, Q. Zhou, E. Toska, J. Galeas, A.A. Ku, R.P. Koche, S. Bandyopadhyay, M. Scaltriti, C.B. Lebrilla, F. McCormick, S.E. Kim, UDP-glucose pyrophosphorylase 2, a regulator of glycogen synthesis and glycosylation, is critical for pancreatic cancer growth, Proc. Natl. Acad. Sci. U. S. A. 118 (2021), https://doi.org/10.1073/PNAS.2103592118.
[47] M. Hengstschläger, M. Rosner, M. Fountoulakis, G. Lubec, The cellular response to ectopic overexpression of the tuberous sclerosis genes, TSC1 and TSC2: a proteomic approach, Int. J. Oncol. 27 (2005) 831–838. https://pubmed.ncbi.nlm.nih.gov/16077935/. accessed March 17, 2022.
[48] S.K. Hindupur, M. Colombi, S.R. Fuhs, M.S. Matter, Y. Guri, K. Adam, M. Cornu, S. Piscuoglio, C.K.Y. Ng, C. Betz, D. Liko, L. Quagliata, S. Moes, P. Jenoe, L. M. Terracciano, M.H. Heim, T. Hunter, M.N. Hall, The protein histidine phosphatase LHPP is a tumour suppressor, Nature. 555 (2018) 678–682, https://doi.org/10.1038/nature26140.
[49] D. Bassetti, H.J. Luhmann, S. Kirischuk, Effects of mutations in TSC genes on neurodevelopment and synaptic transmission, Int. J. Mol. Sci. 22 (2021), https://doi.org/10.3390/IJMS22147273.
[50] K. Toriumi, M. Miyashita, K. Suzuki, K. Tabata, Y. Horiuchi, H. Ishida, M. Itokawa, M. Arai, Role of glyoxalase 1 in methylglyoxal detoxification-the broad player of psychiatric disorders, Redox Biol. 49 (2022), https://doi.org/10.1016/J.REDOX.2021.102222.
[51] P. Maher, Methylglyoxal, advanced glycation end products and autism: is there a connection? Med. Hypotheses 78 (2012) 548–552, https://doi.org/10.1016/j.mehy.2012.01.032.
[52] G. Yang, G.I. Cancino, S.K. Zahr, A. Guskjolen, A. Voronova, D. Gallagher, P. W. Frankland, D.R. Kaplan, F.D. Miller, A Glo1-methylglyoxal pathway that is perturbed in maternal diabetes regulates embryonic and adult neural stem cell pools in murine offspring, Cell Rep. 17 (2016) 1022–1036, https://doi.org/10.1016/J.CELREP.2016.09.067.
[53] J. Xie, S.P. de Poi, S.J. Humphrey, L.K. Hein, J.B. Bruning, W. Pan, L.A. Selth, T. J. Sargeant, C.G. Proud, TSC-insensitive Rheb mutations induce oncogenic transformation through a combination of constitutively active mTORC1 signalling and proteome remodelling, Cell. Mol. Life Sci. 78 (2021) 4035–4052, https://doi.org/10.1007/S00018-021-03825-7.
[54] H. Cao, J. Luo, Y. Zhang, X. Mao, P. Wen, H. Ding, J. Xu, Q. Sun, W. He, C. Dai, K. Zen, Y. Zhou, J. Yang, L. Jiang, Tuberous sclerosis 1 (Tsc1) mediated mTORC1 activation promotes glycolysis in tubular epithelial cells in kidney fibrosis, Kidney Int. 98 (2020) 686–698, https://doi.org/10.1016/J.KINT.2020.03.035.
[55] A. Csibi, J. Blenis, Appetite for destruction: the inhibition of glycolysis as a therapy for tuberous sclerosis complex-related tumors, BMC Biol. 9 (2011) 69, https://doi.org/10.1186/1741-7007-9-69.
[56] A.T. Jones, K. Narov, J. Yang, J.R. Sampson, M.H. Shen, Efficacy of dual inhibition of glycolysis and Glutaminolysis for therapy of renal lesions in Tsc2 +/− mice, Neoplasia. 21 (2019) 230–238, https://doi.org/10.1016/J.NEO.2018.12.003.
[57] J. Haapasalo, K. Nordfors, H. Haapasalo, S. Parkkila, The expression of carbonic anhydrases II, IX and XII in brain tumors, Cancers (Basel) 12 (2020) 1–20, https://doi.org/10.3390/CANCERS12071723.
[58] D.A. Annan, N. Maishi, T. Soga, R. Dawood, C. Li, H. Kikuchi, T. Hojo, M. Morimoto, T. Kitamura, M.T. Alam, K. Minowa, N. Shinohara, J.M. Nam, Y. Hida, K. Hida, Carbonic anhydrase 2 (CAII) supports tumor blood endothelial cell survival under lactic acidosis in the tumor microenvironment, Cell. Commun. Signal. 17 (2019), https://doi.org/10.1186/S12964-019-0478-4.
[59] M. Yuksel, F. Ustabas Kahraman, S. Selek, O. Faruk Ozer, A. Iscan, Oxidant and antioxidant levels and DNA damage in tuberous sclerosis, Brain Dev. 41 (2019) 245–249, https://doi.org/10.1016/J.BRAINDEV.2018.10.014.
[60] X. Fu, X. Sun, L. Zhang, Y. Jin, R. Chai, L. Yang, A. Zhang, X. Liu, X. Bai, J. Li, H. Wang, J. Gao, Tuberous sclerosis complex-mediated mTORC1 overactivation promotes age-related hearing loss, J. Clin. Invest. 128 (2018) 4938–4955, https://doi.org/10.1172/JCI98058.
[61] S. Chakraborty, E. Sircar, C. Bhattacharyya, A. Choudhuri, A. Mishra, S. Dutta, S. Bhatta, K. Sachin, R. Sengupta, S-Denitrosylation: A crosstalk between glutathione and Redoxin systems, Antioxidants (Basel) 11 (2022) 1921, https://doi.org/10.3390/ANTIOX11101921.
[62] S.I. Okamoto, S.A. Lipton, S-Nitrosylation in neurogenesis and neuronal development, Biochim. Biophys. Acta 2015 (1850) 1588–1593, https://doi.org/10.1016/J.BBAGEN.2014.12.013.
[63] M. Kartawy, I. Khaliulin, H. Amal, Systems biology reveals S-Nitrosylation-dependent regulation of mitochondrial functions in mice with Shank3 mutation associated with autism Spectrum disorder, Brain Sci. 11 (2021), https://doi.org/10.3390/BRAINSCI11060677.
[64] P.T. Filipczak, C. Thomas, W. Chen, A. Salzman, J.D. McDonald, Y. Lin, S. A. Belinsky, TSC2 deficiency unmasks a novel necrosis pathway that is suppressed by the RIP1/RIP3/MLKL signaling Cascade, Cancer Res. 76 (2016) 7130–7139, https://doi.org/10.1158/0008-5472.CAN-16-1052.
[65] S.M. Lee, H.J. Koh, D.C. Park, B.J. Song, T.L. Huh, J.W. Park, Cytosolic NADP+-dependent isocitrate dehydrogenase status modulates oxidative damage to cells, Free Radic. Biol. Med. 32 (2002) 1185–1196, https://doi.org/10.1016/S0891-5849(02)00815-8.
[66] S. Boulos, B.P. Meloni, P.G. Arthur, B. Majda, C. Bojarski, N.W. Knuckey, Evidence that intracellular cyclophilin A and cyclophilin A/CD147 receptor-mediated ERK1/2 signalling can protect neurons against in vitro oxidative and ischemic injury, Neurobiol. Dis. 25 (2007) 54–64, https://doi.org/10.1016/J.NBD.2006.08.012.
[67] J. Suzuki, Z.G. Jin, D.F. Meoli, T. Matoba, B.C. Berk, Cyclophilin A is secreted by a vesicular pathway in vascular smooth muscle cells, Circ. Res. 98 (2006) 811–817, https://doi.org/10.1161/01.RES.0000216405.85080.A6.
[68] S. Yoshida, A. Yamamoto, H. Masumoto, T. Fuchigami, A. Toriba, M. Haratake, M. Nakayama, Peptidyl-prolyl cis-trans isomerase A participates in the selenium transport into the rat brain, J. Biol. Inorg. Chem. 26 (2021) 933–945, https://doi.org/10.1007/S00775-021-01903-6.
[69] Y. Zhang, J. Nicholatos, J.R. Dreier, S.J.H. Ricoult, S.B. Widenmaier, G. S. Hotamisligil, D.J. Kwiatkowski, B.D. Manning, Coordinated regulation of protein synthesis and degradation by mTORC1, Nature. 513 (2014) 440–443, https://doi.org/10.1038/NATURE13492.
[70] J. Zhao, B. Zhai, S.P. Gygi, A.L. Goldberg, mTOR inhibition activates overall protein degradation by the ubiquitin proteasome system as well as by autophagy, Proc. Natl. Acad. Sci. U. S. A. 112 (2015) 15790–15797, https://doi.org/10.1073/PNAS.1521919112.
[71] A. Rousseau, A. Bertolotti, An evolutionarily conserved pathway controls proteasome homeostasis, Nature. 536 (2016) 184–189, https://doi.org/10.1038/NATURE18943.
[72] A. Baudin, A.K. Moreno-Romero, X. Xu, E.E. Selig, L.O.F. Penalva, D.S. Libich, Structural characterization of the RNA-binding protein SERBP1 reveals intrinsic

disorder and atypical RNA binding modes, Front. Mol. Biosci. 8 (2021), https://doi.org/10.3389/FMOLB.2021.744707.

[73] A. Kosti, P.R. de Araujo, W.Q. Li, G.D.A. Guardia, J. Chiou, C. Yi, D. Ray, F. Meliso, Y.M. Li, T. Delambre, M. Qiao, S.S. Burns, F.K. Lorbeer, F. Georgi, M. Flosbach, S. Klinnert, A. Jenseit, X. Lei, C.R. Sandoval, K. Ha, H. Zheng, R. Pandey, A. Gruslova, Y.K. Gupta, A. Brenner, E. Kokovay, T.R. Hughes, Q.D. Morris, P.A. F. Galante, S. Tiziani, L.O.F. Penalva, The RNA-binding protein SERBP1 functions as a novel oncogenic factor in glioblastoma by bridging cancer metabolism and epigenetic regulation, Genome Biol. 21 (2020), https://doi.org/10.1186/S13059-020-02115-Y.

[74] T. Porstmann, C.R. Santos, B. Griffiths, M. Cully, M. Wu, S. Leevers, J.R. Griffiths, Y.L. Chung, A. Schulze, SREBP activity is regulated by mTORC1 and contributes to Akt-dependent cell growth, Cell Metab. 8 (2008) 224–236, https://doi.org/10.1016/J.CMET.2008.07.007.